

General Disclaimer

One or more of the Following Statements may affect this Document

- This document has been reproduced from the best copy furnished by the organizational source. It is being released in the interest of making available as much information as possible.
- This document may contain data, which exceeds the sheet parameters. It was furnished in this condition by the organizational source and is the best copy available.
- This document may contain tone-on-tone or color graphs, charts and/or pictures, which have been reproduced in black and white.
- This document is paginated as submitted by the original source.
- Portions of this document are not fully legible due to the historical nature of some of the material. However, it is the best reproduction available from the original submission.

(NASA-CR-149216) ASTRONOMICAL POLARIZATION
STUDIES AT RADIO AND INFRARED WAVELENGTHS.
PART 2: FAR INFRARED POLARIZATION OF DUST
CLOUDS (Cornell Univ., Ithaca, N.Y.) 51 p
HC A04/MF A01

N77-13959

Unclass

CSCL 03B G3/93 55830

CORNELL UNIVERSITY

Center for Radiophysics and Space Research

ITHACA, N. Y.

CRSR 647

ASTRONOMICAL POLARIZATION STUDIES
AT RADIO AND INFRARED WAVELENGTHS

PART II

FAR INFRARED POLARIZATION
OF DUST CLOUDS

A Thesis

Brian K. Dennison



BIOGRAPHICAL SKETCH

Brian Kenneth Dennison was born on August 14, 1949, in Louisville, Kentucky, the son of Mr. and Mrs. Kenneth G. Dennison. He has a sister, Sarah.

He received a B.S. with Honors in Physics from the University of Louisville in December, 1970. At Cornell University he received an M.S. in August, 1974 and a Ph.D. in Astronomy in September, 1976. He served as a Teaching Assistant and Planetarium Lecturer at the University of Louisville, and as a Teaching Assistant and Research Assistant at Cornell University. He held Summer Research Assistantships with the National Radio Astronomy Observatory and the Sacramento Peak Observatory.

He was married to Mira Pahlic on July 17, 1976.

ACKNOWLEDGMENTS

Numerous scientists and engineers played absolutely essential roles in carrying out the experiments discussed in Part I of this thesis. Martin Harwit, David Jauncey, John Broderick, and Dave Shaffer were involved in the very long baseline observations. John Broderick, R. V. E. Lovelace, Benno Rayhrer, and Joe Burch assisted in the processing of these observations. Richard Schillizzi assisted in the second very long baseline experiment. Unfortunately, this experiment failed, although through no fault of Dr. Schillizzi. He was observing at the Owens Valley Radio Observatory, whereas the failure occurred at the National Radio Astronomy Observatory. Arthur Niell was kind enough to devote a portion of his own long baseline processor time to a preliminary search for interference fringes in this experiment. The intermediate baseline analysis was made possible by the generosity of Ed Fomalont and Richard Sramek who provided us with fringe phases from their gravitational bending experiment. They deserve very special appreciation. John Dickey assisted in these observations. The Helios 1 observations were prepared by Chuck Stelzried and Tak Sato of the Jet Propulsion Laboratory. Dr. Sato was involved (often alone) in carrying out these observations.

Advice concerning various stages of data reduction was provided by Martin Harwit, Dave Jauncey, John Broderick, R. V. E. Lovelace, Barry Clark, Paul Hemmenway, Ed Fomalont, Harry Hardebeck, and

Ken Kellerman. Concerning the basic ideas of this study, I wish to thank Stuart Shapiro, Saul Teukolski, R. V. E. Lovelace, E. E. Salpeter, R. V. Wagoner, and especially Martin Harwit for valuable discussions. Barry Clark, Jim Condon, and Thomas Gold all suggested, in some form or another, the concept of using the relative phase delay between orthogonal polarizations. I thank Dr. M. K. Bird, of the Radioastronomisches Institut Univ. Bonn, for providing a preprint concerning the Faraday rotation experiment in advance of publication.

The research carried out in Part I was supported by grants from the National Science Foundation, the Research Corporation, and the National Aeronautics and Space Administration. I also acknowledge support in various forms from the National Radio Astronomy Observatory, the National Astronomy and Ionosphere Center, and the Jet Propulsion Laboratory. The National Radio Astronomy Observatory is operated by Associated Universities, Inc., under contract with the National Science Foundation. The National Astronomy and Ionosphere Center is operated by Cornell University, under contract with the National Science Foundation.

Like the first part of this thesis, the work discussed in Part II relied upon the professional expertise of various scientists and engineers. The successful performance of the polarimeter can be largely attributed to Dennis Ward, who was heavily involved in every phase of its design, construction, and operation. The basic design of the instrument is his. The preamplifier was designed, and

constructed by Dr. Ward. I thank George Gull, and Dennis Ward, and Larry Caroff, and Ed Erickson of NASA Ames Research Center for risking their lives and their eardrums on the observing flights. I am especially thankful since I was unable to fly. Close technical collaboration in the field was provided by Dr. Ward and Mr. Gull. I thank Martin Harwit, Dennis Ward, Bill Forrest, and Jim Elliot for valuable discussions concerning data reduction and systematic effects. Dr. Forrest first suggested the wedge effect problem. For discussions concerning the theoretical aspects of far infrared polarization I thank Martin Harwit, Bill Forrest, and Peter Gierasch. Jerry Stasavage provided excellent technical assistance in the laboratory. The staff of NASA Ames Research Center was helpful in all aspects of the field operation. Some particularly helpful individuals are Bob Mason, Hjal Schacht, Bob Cullum, Calvin Kohl, and Wally Light. Jack Kroupa, the navigator, carefully planned our flights to give optimum observing periods. Without the pilots, the observations would not have been possible. This work was supported by National Aeronautics and Space Administration Contract NGR-33-010-146.

Finally, I thank the members of my special committee, Professors R. V. E. Lovelace, and Yervant Terzian for valuable comments and suggestions. Professor Martin Harwit served as Chairman of my committee, and I thank him for continual advice. The original conceptions of the experiments presented in this thesis are his.

The figures were drawn by Mrs. Barbara Boettcher. The final draft was typed by Mrs. I. Marie Jones.

Parts of this thesis were published in the article, "Gravitational Deflection of Polarized Radiation" by Martin Harwit, R. V. E. Lovelace, Brian Dennison, David L. Jauncey, and John Broderick, which appeared in Nature 249, 230 (1974).

TABLE OF CONTENTS

Page

PART I

Gravitational Deflection of Polarized Radiation.	2
CHAPTER I - GENERAL IDEAS AND THEORY	3
A. Introduction	3
B. Angular Momentum Coupling.	8
C. Coupling with Inhomogeneities in the Gravita- tional Field	11
D. Parity Nonconservation in Gravitation	13
References	19
CHAPTER II- EXPERIMENTS	21
A. General Approaches	21
B. Very Long Baseline Interferometry	25
C. Intermediate Baseline Interferometry	32
D. Relative Phase Shift Technique	40
E. Conclusions.	55
References	59
CHAPTER III-THE FUTURE	61
A. Solar Experiments	61
B. Compact Objects.	63
C. "Large Scale" Compact Objects.	64
D. Conclusions.	66
References	69

	Page
PART II	
Far Infrared Polarization of Dust Clouds. . . .	70
CHAPTER IV - THEORY OF FAR INFRARED POLARIZATION.	71
A. Short Wavelength Polarization	71
B. Long Wavelength Polarization	74
References.	84
CHAPTER V - OBSERVATIONS.	85
A. Initial Experiment.	85
B. Future Experiments	105
C. Conclusions	106
References	107
SUMMARY	108

LIST OF TABLES

	Page
<u>Table I-1</u>	
Theoretical Estimates of the Polarization Splitting.	18
<u>Table II-1</u>	
VLBI Upper Limits to the Polarization Splitting.	35
<u>Table II-2</u>	
Intermediate Baseline Upper Limits to the Polarization Splitting.	41
<u>Table II-3</u>	
Phase Delay Upper Limits to the Polarization Splitting	56
<u>Table II-4</u>	
Established Upper Limits to the Polarization Splitting	57
<u>Table III-1</u>	
Polarization of the Background Radiation by Large Kerr Black Holes.	67

LIST OF FIGURES

	Page
 <u>Figure I-1</u>	
Polarization splitting by gravitational bending.	7
 <u>Figure I-2</u>	
Total internal reflection.	12
 <u>Figure II-1</u>	
The VLBI system.	28
 <u>Figure II-2</u>	
Polarization switching scheme.	29
 <u>Figure II-3</u>	
The source configuration for the VLBI experiment	30
 <u>Figure II-4</u>	
Relative fringe phases between LCP and RCP for 3C 273.	34
 <u>Figure II-5</u>	
The source configuration for the intermediate baseline experiment	38
 <u>Figure II-6</u>	
The polarization of a wave formed by the superposition of two orthogonally polarized waves	44
 <u>Figure II-7</u>	
The positions of the Helios 1 spacecraft relative to the sun during the April (a) and August (b) occultations.	49

	Page
<u>Figure II-8</u>	
Ellipticity scans obtained during the April, 1975	
occultation.	51
<u>Figure II-9</u>	
Ellipticity scans obtained during the August, 1975	
occultation.	52
<u>Figure IV-1</u>	
Theoretical model for producing polarized infrared radiation.	73
<u>Figure IV-2</u>	
Theoretical Polarization of Orion	80
<u>Figure V-1</u>	
Schematic diagram of the polarimeter mounted on the Lear	
telescope.	86
<u>Figure V-2</u>	
Block diagram of the polarimeter electronics	87
<u>Figure V-3</u>	
The wedge effect	91
<u>Figure V-4</u>	
Contour map of the polarimeter beam	93
<u>Figure V-5</u>	
Polarization observations of Venus	94
<u>Figure V-6</u>	
Polarization observations of M42.	97

	Page
<u>Figure V-7</u>	
The wedge effect in visible light.	98
<u>Figure V-8</u>	
Fourier analysis of the Venus data	102
<u>Figure V-9</u>	
Fourier analysis of the Orion data	104

ASTRONOMICAL POLARIZATION STUDIES AT RADIO AND INFRARED WAVELENGTHS

Brian K. Dennison, Ph.D.
Cornell University, 1976

ABSTRACT

In an astrophysical context the polarization of electromagnetic radiation carries important information about the spatial properties of the regions of its origin or those regions through which it has passed. In this thesis two distinct cases are considered.

In Part I the gravitational field is probed in a search for polarization dependence in the light bending. This involves searching for a splitting of a source image into orthogonal polarizations as the radiation passes through the solar gravitational field. This search was carried out using the techniques of very long and intermediate baseline interferometry, and by seeking a relative phase delay in orthogonal polarizations of microwaves passing through the solar gravitational field. In this last technique a change in the total polarization of the Helios 1 carrier wave was sought as the spacecraft passed behind the sun. No polarization splitting was detected, and the most stringent upper limits are $\approx 5 \times 10^{-8}$ arc seconds. This constitutes a unique confirmation of the equivalence principle. Future work involving compact objects may reveal a polarization dependence in the gravitational scattering of electromagnetic

radiation.

Part II of this thesis involves possible far infrared polarization of dust clouds. The recently observed 10 micron polarization of the Orion Nebula and the Galactic Center suggests that far infrared polarization may be found in these objects. Estimates are made of the degree of far infrared polarization that may exist in the Orion Nebula. A first attempt to observe far infrared polarization from the Orion Nebula has been carried out. Future observations will be useful in deducing the detailed structure of dust clouds.

PART II

Far Infrared Polarization of Dust Clouds

CHAPTER IV

THEORY OF FAR INFRARED POLARIZATION

A. Short Wavelength Polarization

Recent observations have uncovered significant linear polarization in the 3-13 micron radiation from the Orion Nebula (Dyck, et al., 1973; Dyck and Beichman, 1974) and the Galactic Center (Dyck, et al., 1974; Capps and Knacke, 1976). In both cases the magnitude of polarization is correlated with the silicate absorption feature, while the polarization direction does not appear to change significantly over this wavelength range. Because of these features it has been argued that this polarization is caused by preferential extinction by aligned dust particles (Dyck and Beichman, 1974; Capps and Knacke, 1976). At these wavelengths the cooler absorbing medium does not radiate appreciably.

The observations of the Orion Nebula (Dyck and Beichman, 1974) are particularly interesting. Their observations were centered on the Becklin-Neugebauer object (BN), an infrared point source, and made over the surrounding Kleinman-Low Nebula (KL). This nebula contains a number of compact objects, in addition to a diffuse component (Rieke, et al., 1973). They observed roughly uniform alignment over the angular extent of their observation ($\sim 1/2^\circ$). The magnitude of the polarization was as large as 15% in the silicate absorption band.

A simple model (Dyck and Beichman, 1974) is illustrated in Figure IV-1. The propagation is in the z-direction, and the x- and y-axes are principal axes. As the rotation angle is varied the optical depth, τ , reaches a maximum value τ_y . The minimum value of τ is τ_x , and this occurs for the orthogonal orientation. Of course, this anisotropy in τ is due to the alignment of elongated dust grains in the cold cloud. The intensity transmitted through the cloud is

$$I_{x,y} = I_0 e^{-\tau_{x,y}}$$

where I_0 is the intensity incident from the hot source. This hot source is optically thick and therefore emits unpolarized radiation. The resulting polarization by absorption is

$$P_a = - \frac{I_x - I_y}{I_x + I_y} = - \frac{e^{-\tau_x} - e^{-\tau_y}}{e^{-\tau_x} + e^{-\tau_y}}.$$

Further simplification results if we define the difference in optical depth,

$$\Delta \tau \equiv \tau_y - \tau_x.$$

Then

$$P_a = - \tanh \left(\frac{\Delta \tau}{2} \right).$$

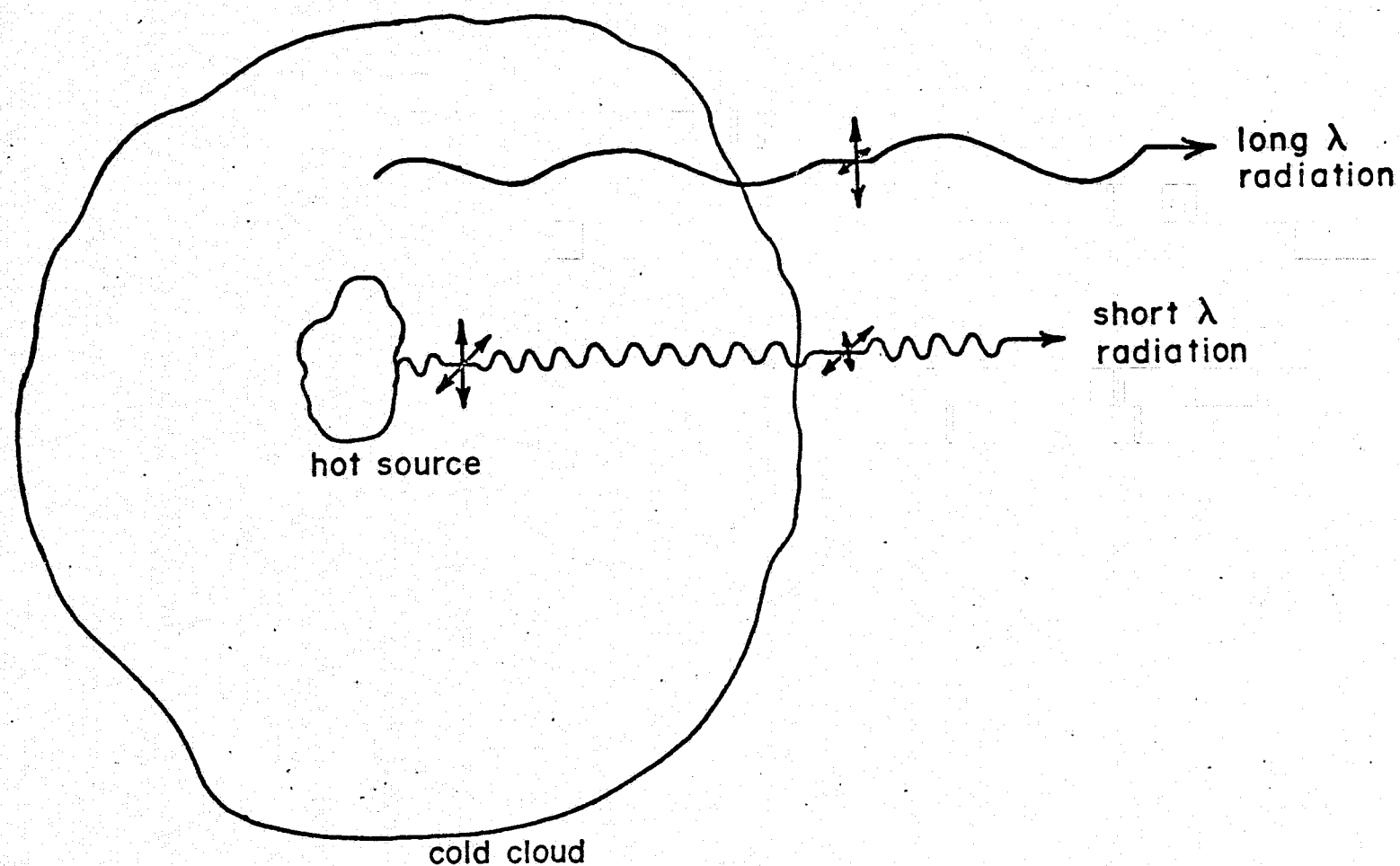


FIGURE IV-1. Theoretical model for producing polarized infrared radiation.

By convention P_a is negative indicating polarization by absorption.

B. Long Wavelength Polarization

At longer wavelengths this cold dust may contribute a significant fraction of the total emission. Therefore, we shall attempt to predict the polarization produced in emission. Initially, we shall just consider the emission by the extended cold cloud. Later, the effect of the hot compact components will be included in the discussion. Including the effects of radiative transfer the intensity emergent from the cloud is

$$I_{x,y} = I_0 (1 - e^{-\tau_{x,y}}),$$

where I_0 is the intensity observed if the source were a blackbody ($\tau_{x,y} \rightarrow \infty$). In this case, the optical depths correspond to the entire thickness of the cloud. The resulting polarization by emission is

$$P_e = - \frac{(1 - e^{-\tau_x}) - (1 - e^{-\tau_y})}{(1 - e^{-\tau_x}) + (1 - e^{-\tau_y})}.$$

We now define the mean optical depth as

$$\langle \tau \rangle \equiv \frac{1}{2} (\tau_x + \tau_y).$$

We then have

$$P_e = \frac{e^{-\langle \tau \rangle} (e^{-\frac{\Delta \tau}{2}} - e^{\frac{\Delta \tau}{2}})}{2 - e^{-\langle \tau \rangle} (e^{\frac{\Delta \tau}{2}} + e^{-\frac{\Delta \tau}{2}})} .$$

This simplifies to

$$P_e = \frac{\sinh \left(\frac{\Delta \tau}{2} \right)}{e^{\langle \tau \rangle} - \cosh \left(\frac{\Delta \tau}{2} \right)} .$$

By definition $\frac{\Delta \tau}{2} < \langle \tau \rangle$. (As long as there is no stimulated emission.) P_e is positive indicating a 90° rotation with respect to the absorption polarization.

A model describing grain alignment is needed to connect $\Delta \tau$ and $\langle \tau \rangle$. The picket fence model (Dyck and Beichman, 1974) gives

$$\tau_{x,y} = \frac{1}{2} \left[(1 + f) Q_{\perp,11} + (1 - f) Q_{11,\perp} \right] G N l .$$

where f is the fraction of totally aligned grains, $Q_{11,\perp}$ are grain extinction efficiencies parallel and perpendicular to the symmetry axis, G is the geometrical cross section of a grain, N is the number density of grains, and l is the path length through the medium. We then find the simple relations

$$\langle \tau \rangle = \frac{1}{2} (Q_{11} + Q_{\perp}) G N l \text{ and } \Delta \tau = f (Q_{11} - Q_{\perp}) G N l .$$

The extinction efficiency of a grain depends on which axis is aligned parallel to the electric vector of the incident radiation. For the j^{th} axis of an ellipsoidal grain we find that (van de Hulst, 1957)

$$Q_j = \frac{1}{3} \frac{a}{\lambda} \Im m \left[\frac{m^2 - 1}{L_j(m^2 - 1) + 1} \right]$$

m is the complex refractive index and L_j is the shape factor for the j^{th} axis. For spheres $L_j = 1/3$, and the usual expression,

$$Q = \frac{a}{\lambda} \Im m \left[\frac{m^2 - 1}{m^2 + 2} \right],$$

is recovered. If we define $m^2 \equiv \epsilon' + i\epsilon''$ then

$$Q_j = \frac{1}{3} \frac{a}{\lambda} \Im m \left[\frac{\epsilon' + i\epsilon'' - 1}{L_j(\epsilon' + i\epsilon'' - 1) + 1} \right].$$

Eventually we obtain

$$Q_j = \frac{1}{3} \frac{a}{\lambda} \left[\frac{\epsilon''}{(L_j(\epsilon' - 1))^2 + (L_j\epsilon'')^2} \right].$$

At short wavelengths Q_j is a complicated function of λ because of resonances in ϵ' and ϵ'' . However, at long wavelengths ($\lambda \gtrsim 40$ microns) ϵ' and ϵ'' may take on the simple behavior $\epsilon' \approx 4$; $\epsilon'' \approx 50$ microns/ λ (microns), based upon studies of lunar dust (Perry, et al.,

1972).

We can now use the short wavelength polarization for the Orion Nebula to predict the long wavelength polarization. Dyck and Beichman (1974) were able to fit their data with a model involving prolate spheroids with an axis ratio of 0.2 and $f \approx 1/4$. From van de Hulst (1957) this gives $L_1 = 0.056$ and $L_2 = L_3 = 0.472$. Then

$$Q_{11} = Q_1 = \frac{1}{3} \frac{a}{\lambda} \left[\frac{\epsilon''}{(0.056 (\epsilon' + 1) + 1)^2 + (0.056 \epsilon'')^2} \right]$$

and

$$Q_{\perp} = Q_2 = Q_3 = \frac{1}{3} \frac{a}{\lambda} \left[\frac{\epsilon''}{(0.472 (\epsilon' - 1) + 1)^2 + (0.472 \epsilon'')^2} \right]$$

The optical depth difference can now be written in terms of the optical depth.

$$\frac{\Delta \tau}{2} = \langle \tau \rangle f \frac{(Q_{11} - Q_{\perp})}{(Q_{11} + Q_{\perp})}.$$

The second term in the denominator of the expressions for the Q_j 's, $((L_j \epsilon'')^2)$, can be neglected since it is small compared to the other term, $((L_j (\epsilon' - 1) + 1)^2)$. This gives $\frac{\Delta \tau}{2} \approx 0.15 \langle \tau \rangle$ independently of wavelength. All that we now need to calculate P_e is $\langle \tau \rangle$ ($\approx \tau$). The cloud may become optically thin at $\lambda \approx 30$ microns (Forrest, et al., 1976; Werner, et al., 1976). For $Q \propto \lambda^{-2}$ the resulting polarization

is given in Figure IV-2 as a function of wavelength.

Several features of the curve can be easily understood. For short wavelengths the source is becoming optically thick as the polarization decreases. As $\tau \rightarrow \infty$, $P_e \rightarrow 0$. For long wavelengths $\tau \rightarrow 0$, and in this limit we have

$$P_e \approx \frac{\Delta \tau/2}{1 + \tau - 1} = \frac{\Delta \tau/2}{\tau}$$

neglecting terms of order τ^2 or higher. We have calculated that $\frac{\Delta \tau}{2}/\tau \approx .15$, and that is the long wavelength limit approached by the curve in Figure IV-2.

Dyck and Beichman (1974) used a model in which the optical depth to BN in the silicate absorption feature is $\tau_{10 \mu} \approx 1.4$. However, Aitken and Jones (1973) and Gillett, et al. (1975) favor interpretations of the absorption spectra which give $\tau_{10 \mu} \approx 3.3$. In Section A it was shown that $P_a = -\tanh\left(\frac{\Delta \tau}{2}\right)$, hence the 10 micron polarization observations fix the value of $\frac{\Delta \tau_{10 \mu}}{2}$. Now the relation

$$\frac{\Delta \tau}{2} = \langle \tau \rangle f \frac{Q_{11} - Q_{\perp}}{Q_{11} + Q_{\perp}}$$

applies generally. Therefore, $\tau_{10 \mu} \approx 3.3$ implies a smaller value for the fractional alignment. Hence, alternative models in which $f \approx 1/10$ will also be considered. The resulting $P_e(\lambda)$ curve is

FIGURE IV-2

Theoretical polarization of Orion. Upper (positive) curves correspond to polarization by emission, with $f = 1/4$ (solid line) and $f = 1/10$ (dotted line). Lower (negative) curves are the combined effect of a hot source seen through the cold cloud. The following sets of parameters were used: $f=1/10$, $T_1 = 75^\circ$ ($\dots - \dots - \dots$), $T_1 = 50^\circ$ ($\cdot - \cdot - \cdot -$); $f=1/4$, $T_1 = 75^\circ$ (-----), $T_1 = 50^\circ$ (— - — - —). T_1 is the temperature of the cold cloud. The hot source was assumed to be at 100°K .

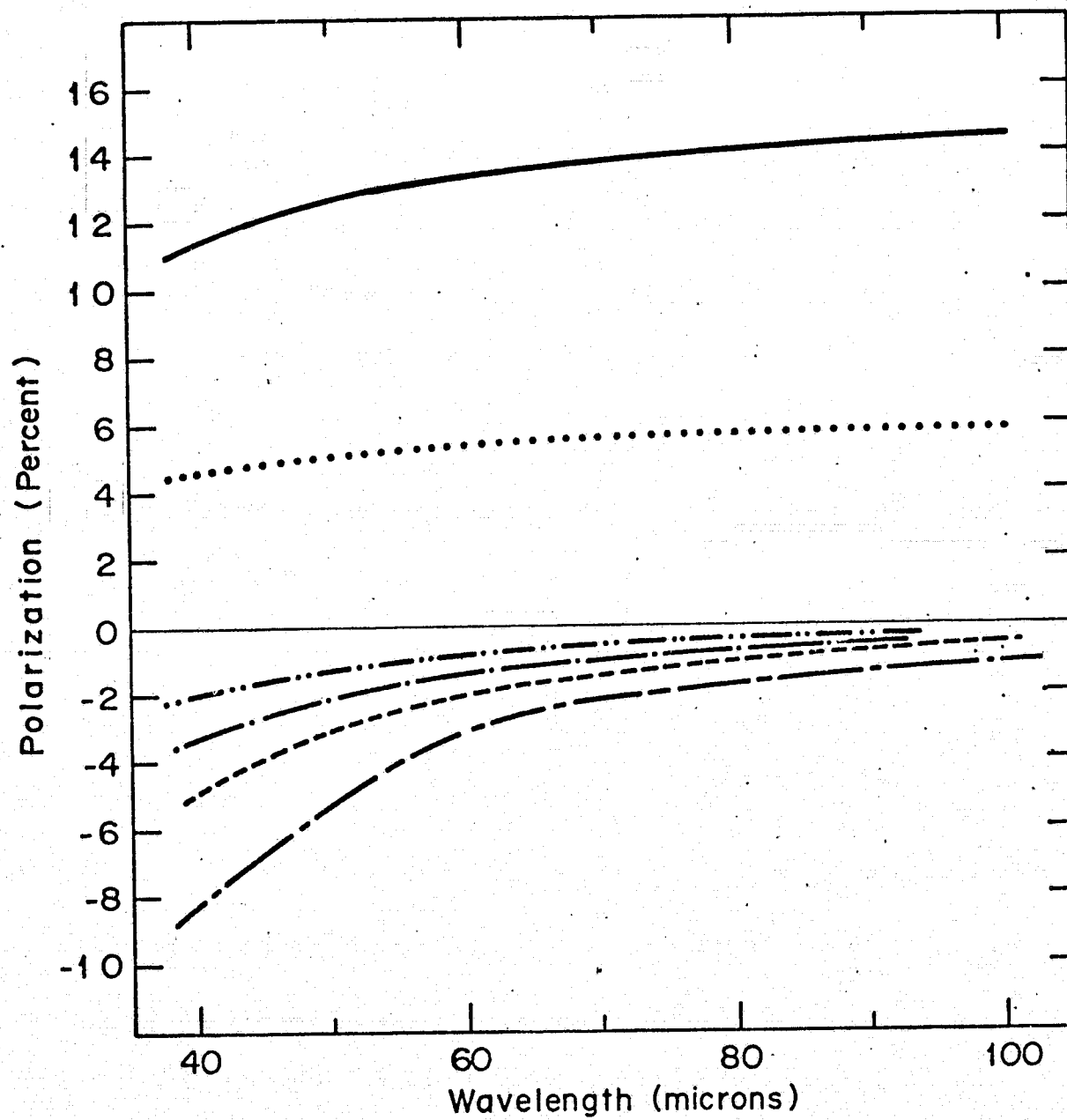


FIGURE IV-2

also shown in Figure IV-2. In this case the long wavelength polarization is $P_e(\lambda = \infty) \approx .06$.

These estimates are also subject to beam size effects and depth effects. If the source is optically thin at long wavelengths, then grain alignment must be maintained through the entire depth of the source, not just down to the hot 10 micron source seen by Dyck and Beichman.

In the foregoing it has been assumed that the source is isothermal. However, because of the present lack of data a detailed model for the radiation transfer is not yet warranted. As a simple case a two-layer model with a hot optically thick region seen through a cooler surrounding medium was considered. Indeed, it has been suggested that numerous clumps optically thick out to 400 microns can produce the observed spectrum (Houck, et al., 1974). In the direction of a hot optically thick underlying region the total emergent intensity is

$$I_{x,y} = B_0 e^{-\tau_{x,y}} + B_1 (1 - e^{-\tau_{x,y}})$$

where B_0 is a Planck function for the temperature of the hot optically thick region, and B_1 is the Planck function for the temperature of the surrounding medium. $\tau_{x,y}$ are the optical depths to the interface separating the regions. The polarization in this direction is

$$P = - \frac{B_0 e^{-\tau_x} + B_1 (1 - e^{-\tau_x}) - B_0 e^{-\tau_y} - B_1 (1 - e^{-\tau_y})}{B_0 e^{-\tau_x} + B_1 (1 - e^{-\tau_x}) + B_0 e^{-\tau_y} + B_1 (1 - e^{-\tau_y})}$$

$$P = - \frac{(B_0 - B_1) e^{-\langle \tau \rangle} \left(e^{\frac{\Delta \tau}{2}} - e^{-\frac{\Delta \tau}{2}} \right)}{2 B_1 + (B_0 - B_1) e^{-\langle \tau \rangle} \left(e^{\frac{\Delta \tau}{2}} + e^{-\frac{\Delta \tau}{2}} \right)}$$

This simplifies to

$$P = \frac{\sinh \left(\frac{\Delta \tau}{2} \right)}{- \frac{B_1}{B_0 - B_1} e^{-\langle \tau \rangle} - \cosh \left(\frac{\Delta \tau}{2} \right)}$$

When $B_1 \rightarrow 0$, the previous expression for the absorption polarization is recovered; and when $B_0 \rightarrow 0$, we obtain the expression for the emission polarization.

In evaluating $P(\lambda)$ it was assumed that the temperature of the underlying region is 100°K . Four models were considered. We used $f = 1/4$ and $f = 1/10$, and considered the temperature of the extended region to be 50°K and 75°K . The resulting curves are given in Figure IV-2. The extended region was assumed to have $\tau \approx 1$ at $\lambda = 30$ microns, and $Q \propto \lambda^{-2}$. Polarization by absorption dominates and this is greatest for $f = 1/4$ and 50°K for the temperature of the extended region.

The observations may include in the beam both regions with and without an underlying hot source. The observed polarization

would then be an appropriately weighted sum of the upper and lower curves in Figure IV-2. Integration over the instrumental bandwidth may also be necessary.

Whether polarization by absorption or emission is the dominant process can be distinguished observationally, through comparison of the polarization direction with that of the 10 micron polarization. In this way long wavelength polarization observations will be of considerable value in deducing the optical depth structure of dust clouds. Of particular interest would be polarization observations over a range of wavelengths.

PART II

CHAPTER IV - REFERENCES

- Aitken, D. K., and Jones, B., Ap. J. 184, 127 (1973).
- Capps, R. W., and Knacke, R. F., preprint 1976.
- Dyck, H. M., and Beichman, C. A., Ap. J. 194, 57 (1974).
- Dyck, H. M., Capps, R. W., and Beichman, C. A., Ap. J. Letters 188, L103 (1974).
- Dyck, H. M., Capps, R. W., Forrest, W. J., and Gillett, F. C., Ap. J. Letters 183, L99 (1973).
- Forrest, W. J., Houck, J. R., and Reed, R. A., preprint 1976.
- Gillett, F. C., Forrest, W. J., Merrill, K. M., Capps, R. W., and Soifer, B. T., Ap. J. 200, 609 (1975).
- Houck, J. R., Schaack, D. F., and Reed, R. A., Ap. J. Letters 193, L193 (1974).
- van de Hulst, H. C., Light Scattering by Small Particles, Wiley & Sons (1957).
- Perry, C. H., Agrawal, D. K., Anastassakis, E., Lowndes, R. P., Rastogi, A., and Tornberg, N. E., The Moon, 4, 315 (1972).
- Rieke, G. H., Low, F. J., and Kleinmann, D. E., Ap. J. Letters 186, L7 (1973).
- Werner, M. W., Gatley, I., Harper, D. A., Becklin, E. E., Loewenstein, R. F., Telesco, C. M., and Thronson, H. A., Ap. J. 204, 420 (1976).

CHAPTER V

OBSERVATIONS

A. Initial Experiment

In the hope of detecting long wavelength polarization from the Orion Nebula a series of long wavelength polarization observations were undertaken. The observations were carried out with the NASA Lear Jet 30-cm telescope, from an altitude of 13.7 km. At this altitude the aircraft was above the tropopause thus minimizing the effects of atmospheric water vapor absorption. The polarimeter consisted of a rotating wire grid polarizer (Cambridge Physical Sciences IGP 223) mounted immediately in front of a liquid helium cooled photometer. The overall system is shown schematically in Figures V-1 and V-2. The polarimeter employed a Ge:Ga photoconductive detector and the bandpass extended from 60 microns to 130 microns, with the short wavelength cutoff produced by a BaF_2 filter, and the long wavelength cutoff by the detector itself. The effective band center was ≈ 85 microns. A field optical system was designed by Dr. Dennis Ward to produce a flat beam profile, thus minimizing guiding errors.

The polarizer was rotated with a stepping motor, and in this way the orientation was known at all times. This was also monitored with a continuous potentiometer connected to the gear train. The wire grid in the polarizer is embedded in a polyethylene substrate,

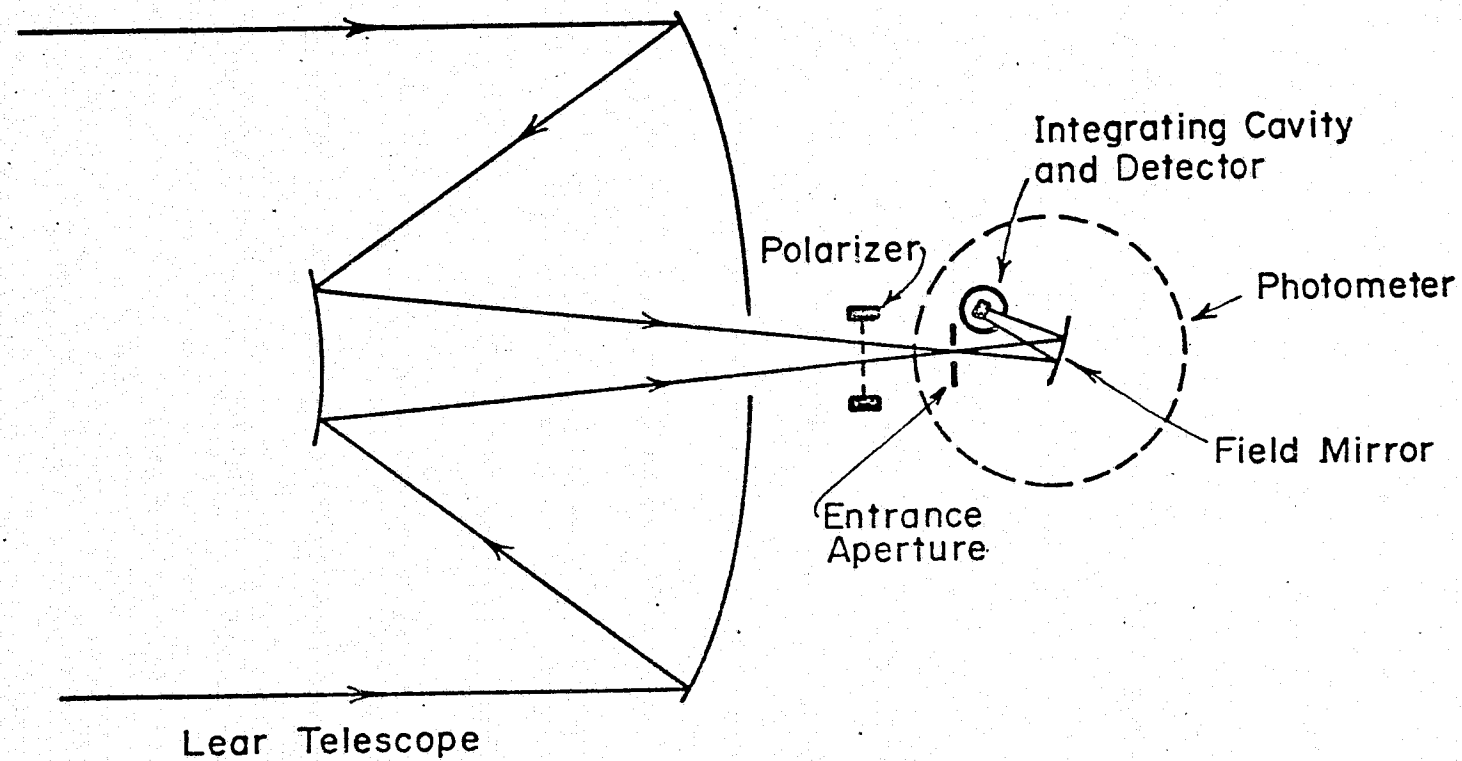


FIGURE V-1. Schematic diagram of the polarimeter mounted on the Lear telescope.

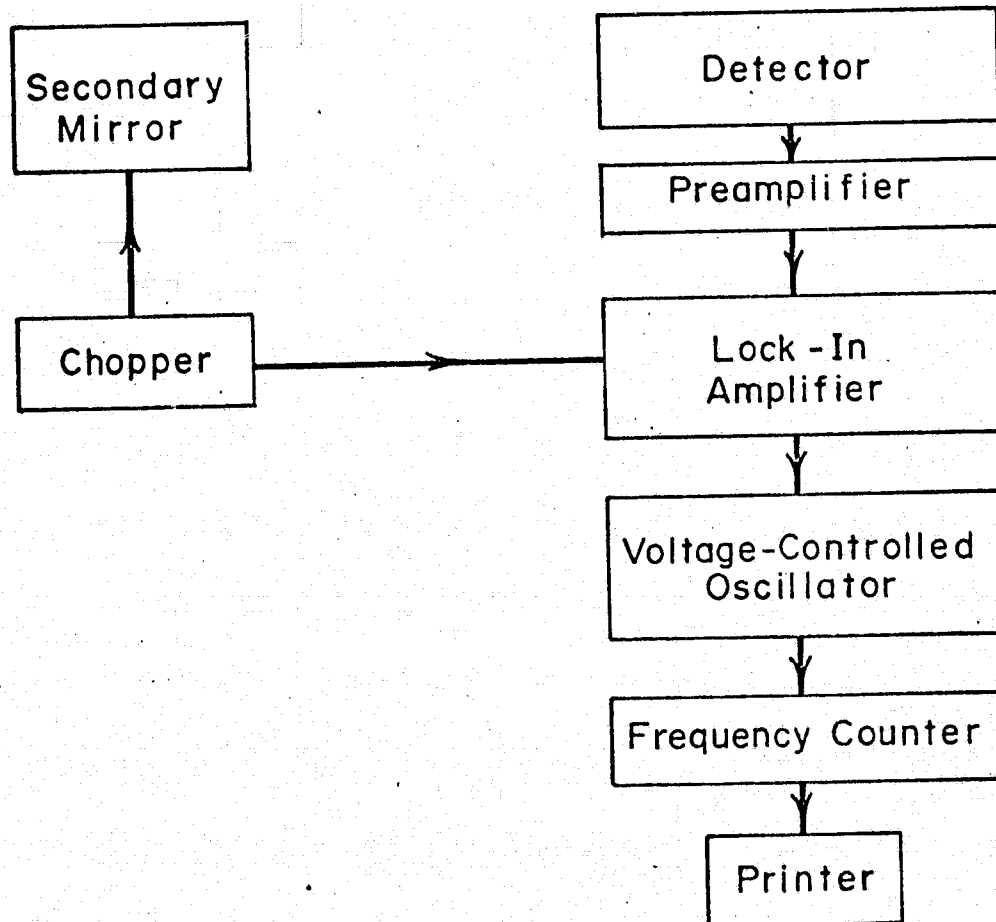


FIGURE V-2. Block diagram of the polarimeter electronics.

and the orientation of the lines is not immediately obvious. Subsequent to the observations the absolute orientation of the polarizer in the "zero" position was accurately measured by diffracting visible laser light through the lines. First and second order diffraction spots were observed displaced in a direction perpendicular to the lines. At long infrared wavelengths a wave with the electric vector perpendicular to the lines is transmitted most readily. This measurement was repeated at three different radial locations in the polarizer. In this way it was seen that the orientation of the lines was uniform. The magnitude of the diffraction angle gives the spacing of the lines. Throughout the polarizer this did not appear to vary by more than a few percent.

The polarimeter was tested by operating it attached to a telescope simulator. The beam was chopped between 77°K (liquid nitrogen) and 300°K (room temperature). The instrumental polarization was measured by observing an unpolarized source, and rotating the polarizer. This was found to be $\approx 2.5\%$. The instrumental polarization is probably due to the non-normal incidence of radiation impinging upon the detector. This geometry was originally employed to make effective use of the integrating cavity. The angle of incidence at the field mirror is $\approx 11^\circ$. This produces much less than a percent of instrumental polarization at these wavelengths (Dall'oglio, et al., 1974). Since two polarizers were purchased it was possible to measure how much radiation was transmitted

when the electric vector is parallel to the lines. This was accomplished by comparing the signal with the polarizers crossed with that obtained when they were aligned. This gave $\sim 4\%$.

With the polarimeter attached to the Lear telescope, the beamwidth was $\sim 6'$. During the observations the beam was chopped on and off the source at a frequency of 30Hz. This was accomplished with a wobbling secondary mirror. The chopper throw was $8'$. The signal was synchronously demodulated with a lock-in amplifier. The lock-in amplifier output fed a voltage controlled oscillator, and the frequency was then counted over the integration time to provide a digital signal. The telescope was initially pointed to maximize the far infrared signal, with polarizer in the "zero" position. The telescope was then gyrostabilized and the observer maintained the positioning by offset guiding on nearby star. Because the observing platform is not thoroughly steady, guiding errors are the dominant form of noise. The polarizer was rotated through 80° intervals and 4 second integrations were carried out at each position. After 9 such rotations the polarizer was back in the original position, resulting in a series of measurements spaced at 40° intervals. This procedure was adapted to minimize any systematic effects of drifts due to guiding noise.

To eliminate the telescope offset signal, this procedure was repeated with the telescope pointed about $15'$ away from the source along a direction perpendicular to the chopper throw. The offset,

runs were then subtracted from temporally adjacent runs on the source. The source and offset runs were alternated throughout the observations.

To calibrate the total instrumental polarization (telescope + polarimeter), Venus was observed on each flight.

Another significant instrumental effect was caused by the polarizer, apparently due to a slight gradient in thickness across its cross section. As the polarizer was rotated the image of a celestial source described a small circular trajectory in the focal plane. This is illustrated schematically in Figure V-3. Image motion in and out of the entrance aperture then produces signal variations as the polarizer is rotated. Fortunately this effect manifests itself primarily over a 360° rotation of the polarizer, whereas source polarization exhibits a 180° period. Therefore, this "wedge effect" is at least partially separable. We note, however, that asymmetries in the beam and source structure could produce signal variations in the second harmonic, which would mimic source polarization.

To fully understand this effect a series of laboratory experiments were undertaken. Firstly, the polarimeter was mounted on an optical bench which simulated far infrared observations with the same f-cone as that from the Lear telescope. Observations of sources of varying angular size could then be simulated by placing different apertures over the far infrared laboratory source. By moving a very

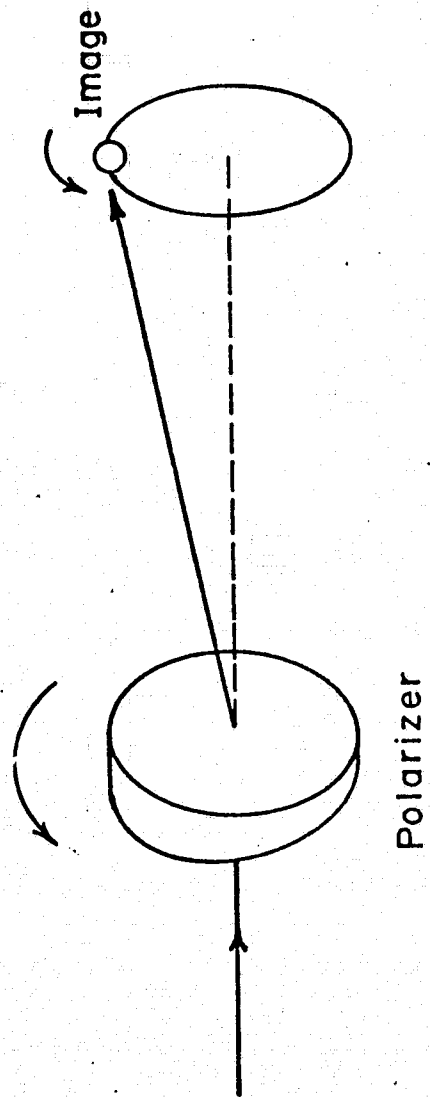


FIGURE V-3. The wedge effect.

small aperture in its plane the beam profile could be probed. In this way the beam was mapped with the polarizer in the zero position, and rotated through 180° . To avoid systematic differences between the two beam maps, each array element was measured first with the polarizer in the zero position, and then with the polarizer rotated through 180° . The resulting maps are basically identical except for one important feature - there is $\sim 1'$ shift in position between the maps. The zero position map is shown in Figure V-4. The beam center is marked, as in the corresponding beam center of the 180° map. The $1'$ displacement is obvious.

Since the displacement is $\sim 1/5$ the beam size, we see that a point source could be kept in the beam as the polarizer is rotated. To test this a small source ($\leq 1'$) was peaked-up in the beam and a series of measurements were made at 40° intervals. The resulting curve reflects only the instrumental polarization. (See Figure V-5.) We then expect that Venus, a source of small angular size, would not be severely affected.

Another feature of the beam map is apparent. It is not circularly symmetric. Thus, as an extended source follows a $1'$ circular trajectory through this beam variation in the signal, in the second and higher harmonics may occur.

Therefore, observations were simulated with an extended source of about the same size as the Orion Nebula $\sim 5'$. For a source with a size comparable to the beam the "wedge effect" should

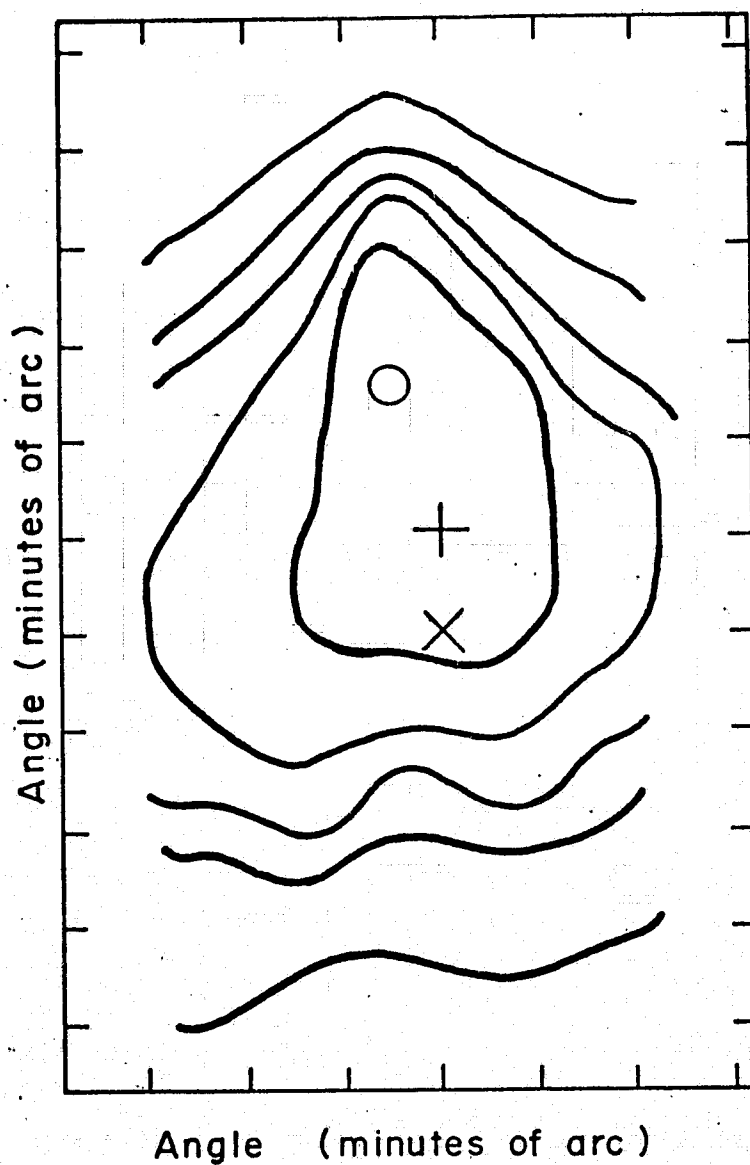


FIGURE V-4.

Contour map of the polarimeter beam. The contour interval is uniform, and all contours above the zero level are shown. The beam center is marked (+). The corresponding location in the map obtained with the polarizer rotated through 180° is also shown (X).

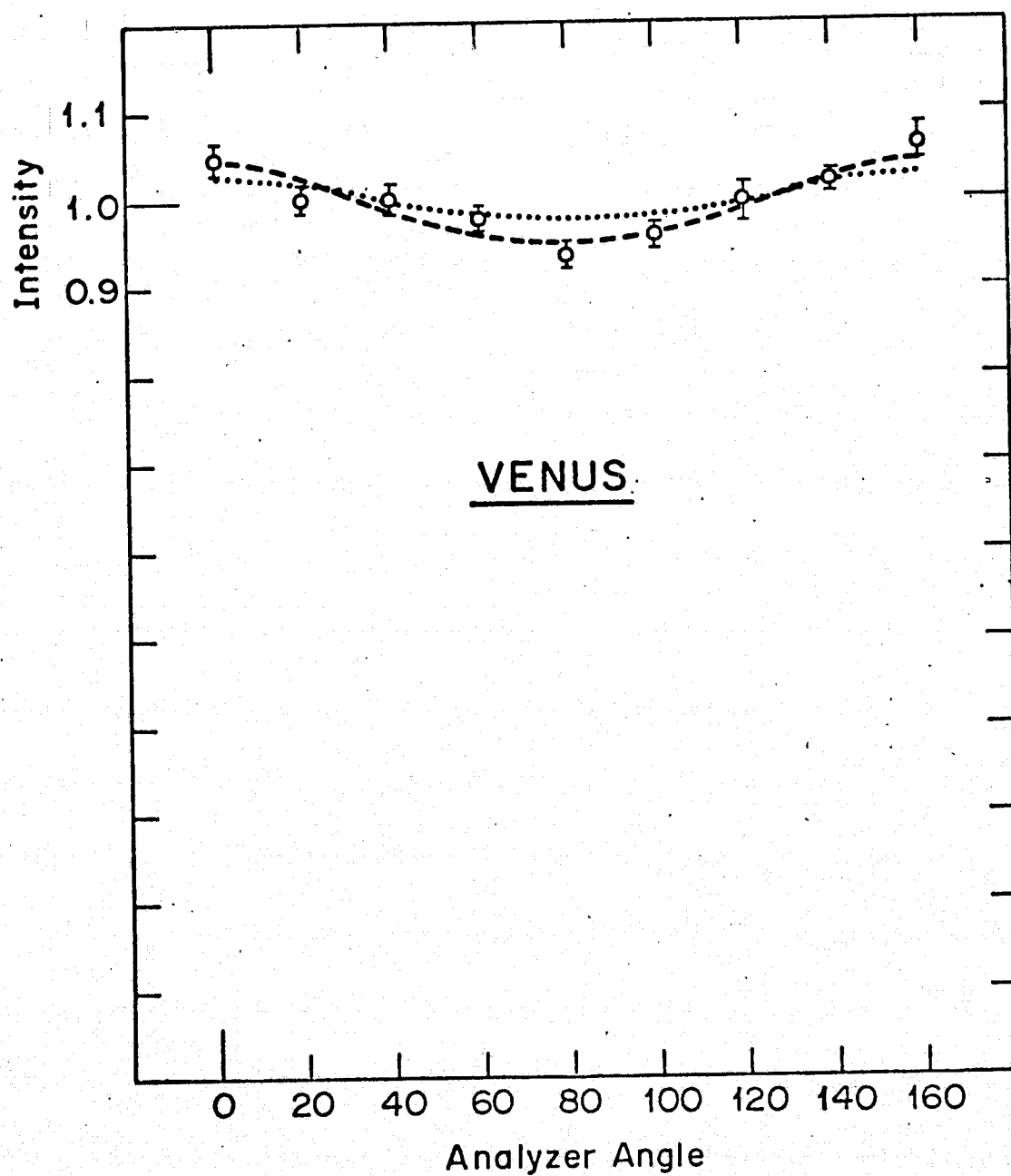


FIGURE V-5

Polarization observations of Venus. Dashed line is the best fit to the data. Dotted line is a laboratory simulation of observations of a point source.

be most pronounced. These simulations were done twice for slightly different initial positionings of the source in the beam. The resulting curves were dominated by a large amplitude fluctuation with 360° period. To determine the relative strength of the "wedge effect" in the all-important second harmonic, this 360° -period component was isolated and removed by Fourier analysis. The results are shown in Figure V-6. Although these curves are of small amplitude, they differ from the instrumental polarization curves by typically $\sim 4\%$. This then dictates the accuracy of the Orion measurements.

Another simulation was carried out with the extended source very poorly positioned in the beam. This curve is also shown in Figure V-6 with the fundamental component removed. The amplitude in the second harmonic is $\sim 8\%$. The pointing accuracy of the real observations is far better than what was simulated in this case.

As the final confirmation of this effect measurements were made at optical wavelengths. A laser beam was passed through the polarizer. As the polarizer was rotated the laser spot followed a circular trajectory on a distant screen. The paths of spot are shown for the two polarizers in Figure V-7. The distance displacement has been calibrated in terms of an angular displacement. This was done with the laser directed through the center, edges, and intermediate location in the polarizers. The angular displacement produced by the instrument polarizer agrees with the $\sim 1/5$ entrance aperture motion implied by Figure V-4. This angular deflection

FIGURE V-6

Polarization observations of M42. Upper horizontal scale denotes position angle on the sky. Arrow indicates approximate position angle of 11 micron polarization observed by Dyck and Beichman (1974). Solid line is the best fit to the data, and the dashed line is the Venus curve. Dotted lines are laboratory simulations of observations of sources with the same angular extent as M42. The large amplitude curve was obtained when the source and beam were intentionally misaligned.

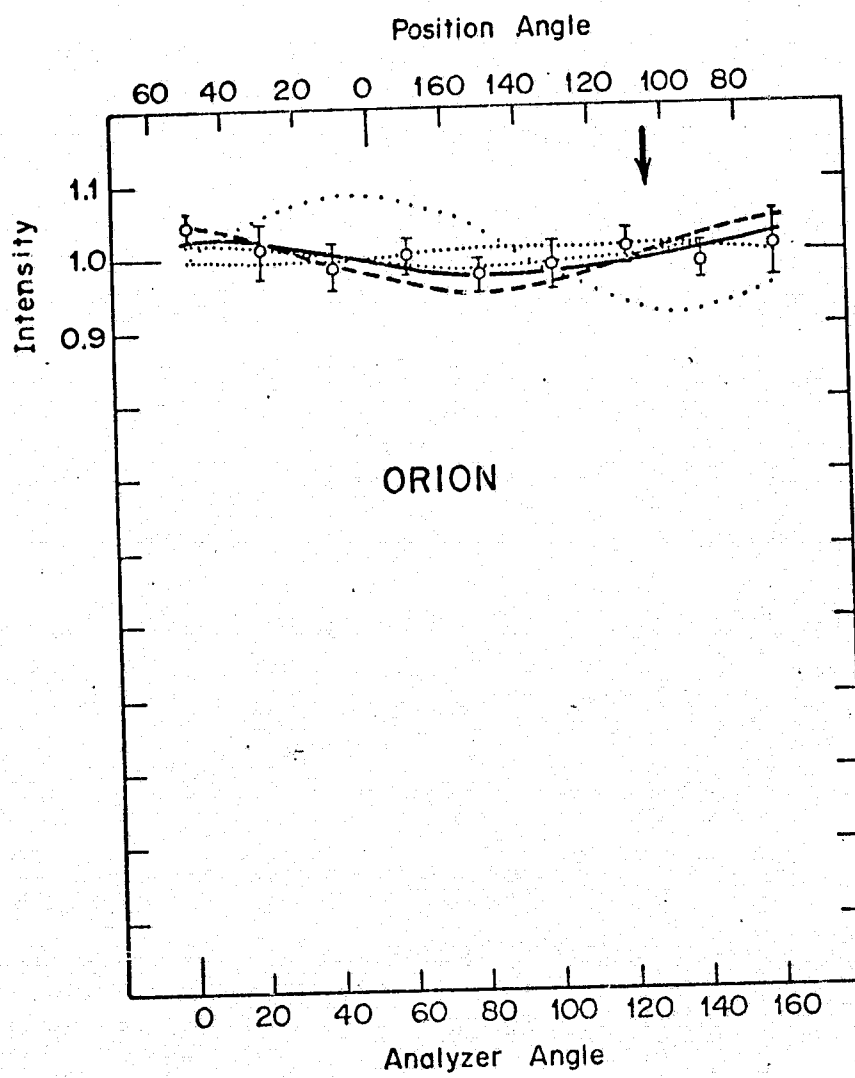








FIGURE V-6

<u>Position</u>	<u>Instrument Polarizer</u>	<u>Lab Polarizer</u>
Center		
Medium		
Edge		

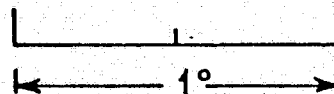


FIGURE V-7

The wedge effect in visible light. The trajectory of a laser beam as a result of polarizer rotation is shown. This was done for 3 locations in each polarizer. For the instrument polarizer the beam position at 40° intervals is shown. The lab polarizer has a much smaller wedge effect, and the beam trajectory is simply shown.

indicates a thickness difference of $\sim 1/10$ mm across the 25 mm diameter of the polarizer. It is noteworthy that the lab(extra) polarizer has a wedge effect about three times smaller than the instrument polarizer.

The Orion Nebula and Venus were observed on three successive flights on December 9, 10, and 11, 1975. For each run (each consisting of integrations at the eight polarizer positions) offsets were removed, and the amplitude normalized. The data taken over the three flights was then combined for each source. The results for Venus and the Orion Nebula are shown in Figures V-5, and V-6, respectively. The Fourier component of period 360° , which is due to the "wedge effect", has been removed in both cases. If we assume that Venus is unpolarized the total instrumental polarization is $\sim 5\%$ peaking at a phase angle $\sim 170^\circ$. The instrumental polarization measured in the laboratory without the Lear telescope was the same phase but is smaller in amplitude. The best fit to the Venus data is shown by the dashed curves (in both Figures V-5 and V-6).

The data from the Orion Nebula is plotted in Figure V-6. The best fit to the data is shown by the solid line. After correcting for the instrumental polarization the net polarization is $2.5\% \pm 2.5\%$ peaking at a phase angle $\sim 80^\circ$. This should be considered an upper limit since the laboratory simulations produced curves of

similar amplitude. The positioning of the source within the beam can slightly alter the second harmonic wedge effect curves. This is consistent with the fact that the observed net "polarization" changed by more than the random errors over the three observing flights.

Fourier analyses of the data from each flight are shown graphically in Figures V-8 and V-9. The vectors plotted with their experimental errors representing Fourier components, at phase angle, ϕ . For this analysis a non-linear least squares fit was carried out with the Fourier series suitably defined. The errors in each data point were taken into account in the fitting procedure. The persistent 5% instrumental polarization is obvious in the Venus' second harmonic. In Figure V-9 we first note that the night-to-night variations in the second harmonic of the Orion Nebula data are greater than the errors. Thus, the wedge effect is the dominant factor limiting the experimental accuracy. In the first flight, the fundamental harmonic is fairly small suggesting that the Orion Nebula was well centered in the beam. For this flight the second Fourier component closely reproduces the instrumental polarization obtained from observing Venus.

We conclude, therefore, that the 85 micron polarization measured here is significantly less than the most optimistic predictions calculated in the last chapter.

This can be explained in a number of ways. Firstly, radiative

FIGURE V-8

Fourier analysis of the Venus data. Fourier vectors are shown for the first 3 harmonics for each flight. $\phi = 0$ corresponds to a pure cosine component. Circles depict experimental errors.

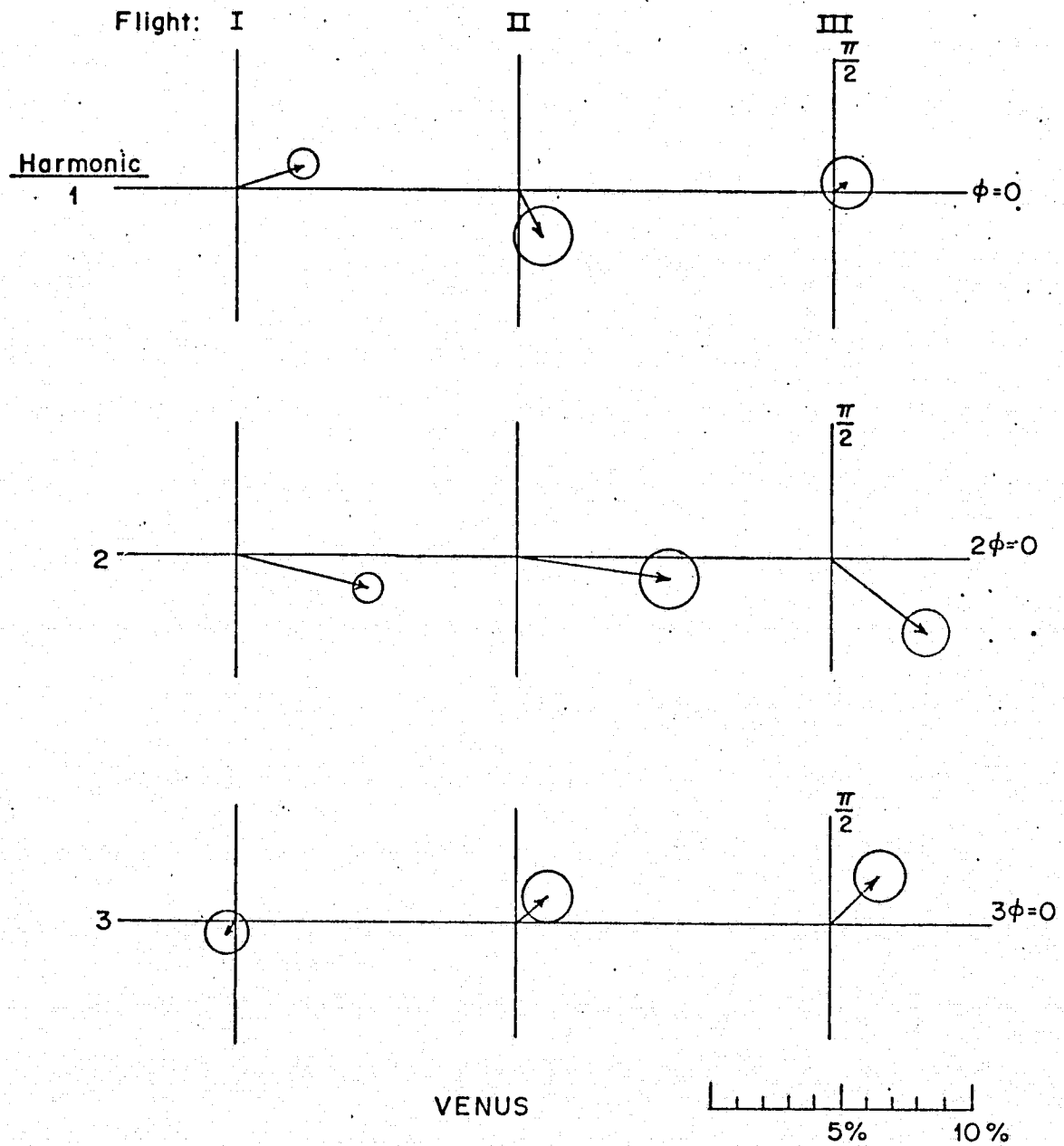


FIGURE V-8

FIGURE V-9

Fourier analysis of the Orion data. Fourier vectors are shown for the first 3 harmonics for each flight. $\phi = 0$ corresponds to a pure cosine component. Circles depict experimental errors.

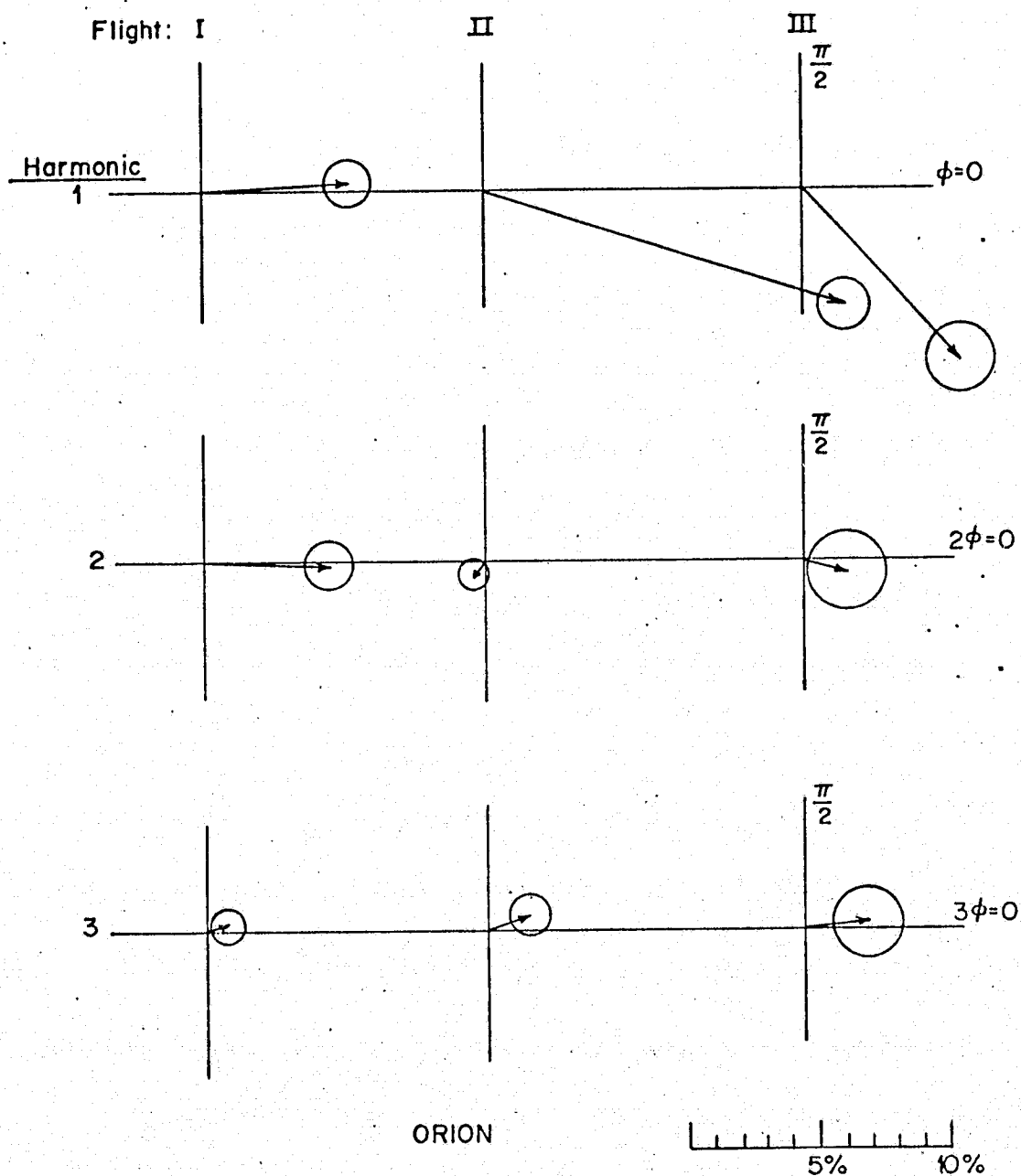


FIGURE V-9

transfer effects in a non-isothermal cloud could account for the lower polarization, as previously discussed.

However, these observations may lack sufficient angular resolution. The 6' beamwidth is considerably larger than the 1/2' beam used by Dyck and Beichman (1974). At 100 microns only about 30% of the flux comes from a 1' region (Werner et al., 1976). Dilution of the 85 micron polarized flux and possibly cancellation effects could have greatly reduced the observed polarization. In the future, higher resolution observations are needed. With this, better guiding accuracy will, of course, be needed.

B. Future Experiments

The need for improved angular resolution dictates that larger aperture telescopes be used, since the Lear jet observations are diffraction limited. The long wavelengths call for highly elevated observing platforms to escape water vapor absorption. In the immediate future the obvious system to use is the C-141 Gerald Kuiper Airborne Observatory operated by NASA. This will provide a factor of three improvement in angular resolution.

With this in mind a few specific suggestions can be made. The wedge effect problem should be evaluated carefully beforehand. It can probably be circumvented by using a polarizer which has been tested and shown to be fairly flat (such as the lab polarizer), and by placing the polarizer as close to the entrance aperture as possible. With the polarizer data presented in Section A the

magnitude of the wedge effect can be determined in the early stages of the preparation.

Also the instrumental polarization can probably be greatly reduced by carefully mounting the detector perpendicular to the incoming beam.

Finally, we note that the instrumental polarization introduced by the 90° reflection in the C-141 telescope should only be $\sim 0.1\%$ (Dall'oglio, et al., 1974). The polarized emission from this mirror should also be small.

Looking farther into the future we can foresee investigations of this sort extended to numerous infrared objects.

C. Conclusions

Long wavelength polarization observations may serve as a new tool for probing the distribution of magnetic fields in dense regions. This will aid in understanding the nature of collapsing regions, and possibly subsequent star formation.

PART II

CHAPTER V - REFERENCES

Dall'oglio, G., Melchiorri, B., Melchiorri, F., Natale, V., Aiello, S., and Mencaraglia, F., in Planets, Stars and Nebulae Studied with Photopolarimetry (T. Gehrels, ed.), pp.322-351. University of Arizona Press (1974).

Dyck, H. M., and Beichman, C. A., Ap. J. 194, 57 (1974).

Werner, M. W., Gatley, I., Harper, D. A., Becklin, E. E., Loewenstein, R. F., Telesco, C. M., and Thronson, H. A., Ap. J. 204, 420 (1976).